Journal of Applied Fluid Mechanics, Vol. 10, No. 5, pp. 1427-1440, 2017.
Available online at www.jafmonline.net, ISSN 1735-3572, EISSN 1735-3645.
DOI: 10.18869/acadpub.jafm.73.242.27229

Massline Visualization of Double-Diffusive Natural Convection inside a Cavity Filled with Nanofluid Subjected to Heat Flux and Transverse Magnetic Field

O. Ghaffarpasand[1,2]

1 Department of Physics, University of Isfahan, Isfahan, Iran
2 Environmental Research Institute, University of Isfahan, Isfahan, Iran

Email: O.ghaffarpasand@gmail.com

(Received September 21, 2016; accepted April 15, 2017)

ABSTRACT

In the present work, massline visualization technique as an innovative method is utilized to deepen our insights into the problem of double-diffusive natural convection of nanofluids. The effects of inclination angle and strength of the external magnetic field on one side and heat flux coefficient on the other side on the masslines, isoconcentrations, isotherms, heat and mass transfer are fairly studied and discussed. The governing equations together with appropriate boundary conditions are solved numerically using a finite difference method in a square lid-drive cavity filled with Cu-water nanofluid. Four pertinent parameters are studied these; the orientation angle of the magnetic field ($\lambda = 0^\circ - 270^\circ$), Hartman number ($Ha = 0 - 100$), heat flux coefficient ($\varepsilon = 1 - 200$), and nanoparticle volume fraction ($\phi = 0 - 10\%$). Results indicate that the orientation and strength of applied magnetic field can be considered as the key parameters in controlling double-diffusive natural convection. It is also found that the existence of metallic nanoparticles in the presence of magnetic field can play different roles in the heat and mass transfer variations. Meanwhile, high amount of heat flux injected through the cavity has an aiding effect on the convective current of mass within the cavity. Results also indicate that nanofluid has relatively smaller massline circulation loops than pure fluid.

Keywords: Double-diffusive natural convection; Nanofluid; Heat flux; Massline visualization technique; Heat and mass transfer.

NOMENCLATURE

B	buoyancy ratio	α	thermal diffusivity
B_0	magnetic field intensity	β	coefficient of thermal expansion
g	gravitational acceleration	ε	heat flux coefficient
Gr	Grashof number	μ	dynamic viscosity
Ha	Hartman number	ν	kinematic viscosity
H	enclosure length	ρ	density
k	thermal conductivity	σ	electrical conductivity
Le	Lewis number	Θ	dimensionless temperature
Nu	local Nusselt number pressure	Φ	dimensionless concentration
P	Prandtl number	ϕ	solid volume fraction
Re	Reynolds number	**Subscript**	
Ri	Richardson number	*f*	pure fluid
Sh	local Sherwood number	s	solid nanoparticles
U_0	upper wall velocity	n*f*	nanofluid
X,Y	dimensionless Cartesian coordinates	T	thermal
		C	solutal

1. INTRODUCTION

The natural convection is driving only by density variations due to temperature gradient, whereas double-diffusive convection as an important fluid dynamics topic is driving by temperature and concentration gradients simultaneously. Double-diffusive convection is frequently encountered in various fields such as metal manufacturing process, ventilations, crystal growth, and oceanography (Schmit, 1994). In such convection, thermal and solutal buoyancies can induce many intriguing and complicated flow, heat and mass transfer phenomena which are important for both of theoretical researches and practical applications (Al-Amiri *et al*. 2007). During the last years, many effective numerical and experimental studies on double-diffusive convection in various regimes, i.e. forced, mixed and natural convections, have been reported in the literature. Among them, Al-Amiri *et al*. (2007) carried out numerical simulations to study the steady mixed thermo-solutal convection in a square lid-driven cavity. Results show that heat transfer is improved by increasing the buoyancy ratio. The double-diffusive flow with horizontal temperature and concentration gradients in a rectangular enclosure was investigated by Qin *et al*. (2013) with a compact difference method with fully fourth-order accuracy and high resolution in space. Jena *et al*. (2014) investigated the transient process of buoyancy-opposed double-diffusive convection of micropolar fluids. Wang *et al*. (2016) utilized a regularized Lattice Boltzmann method (LBM) to con-sider double-diffusive convection in the vertical enclosures. It has been shown that the heat and mass transfer rates are decreased with the increase of the aspect ratio.

An innovative technique to improve the heat transfer of traditional conventional fluids such as water, ethylene glycol, and oil is using the nano-scale particles in the base fluid. Fluids that nanoparticles suspended in them are called nanofluids firstly by Choi (1995). Although the available literature on the double-diffusive natural convection is numerous, the corresponding research utilizing nanofluid as the working fluid is quite sparse. Esfahani & Bordbar (2011) studied numerically the double-diffusive natural convection flow of water-based nanofluids containing various nanoparticles. The effects of the nanoparticles volume fraction, Rayleigh and Lewis numbers on the heat and mass transfer were analyzed in their study. Results reveal that the solutal and thermal transfer rates in the cavity are decreased and increased by increasing the values of the nanoparticles volume fraction, respectively. Parvin *et al*. (2012) performed numerical simulations to analyse double-diffusive natural convection patterns of water-Al_2O_3 nanofluid in a partially heated enclosure. Results clearly demonstrate that the distributions of isotherms and isoconcentrations depend closely on the position of active walls of the cavity. Alim & Nasrin (2013) investigated numerically the double-diffusive natural convection of CuO-water nanofluid in a solar collector. It was indicated that the incident angle of the solar collector affects greatly the performance of heat and mass transfer of nanofluid. Later, Chen *et al*. (2015) conducted entropy generation analyzes on double-diffusive natural convection of nanofluid in a rectangular enclosure. It has been found that the entropy generation of double-diffusive convection of nanofluid is increased significantly in the fully turbulent regimes.

The present literature survey has led us to confirm that there is, relatively, a very little published works regarding the double-diffusive natural convection of nanofluids. Moreover, the topics of nanofluids and magnetic field in the presence of the heat flux have not clearly arisen yet. For electrically conducting fluid, the effect of the Lorenz force is to suppress convection currents by reducing the fluid velocity, so that the presence of an external magnetic field becomes an active control mechanism in manufacturing process (Mondal & Sibanda, 2015). The influence of external magnetic field on the thermo-solutal combined convection has not received significant attention in the literature. Mondal & Sibanda (2015) investigated numerically the effect of buoyancy ratio and external magnetic field on double-diffusive convection of pure air in an inclined rectangular cavity. Results show that fluid flow as well as the temperature and concentration fields are significantly depend on the magnetic field strength and cavity inclination angles. Aly and Raizah (2016) used ISPH method to analyze double-diffusive natural convection in an enclosed filled with nanofluid. Results, show that an increase in Soret number conjugated by a decrease in Dufour number results in an enhancement of heat transfer. Kefayati (2016) utilized the LBM to study double-diffusive natural convection of power-law fluids in the presence of external magnetic field, Soret and Dufour effects in an open cavity. Results indicate that the enhancement of Hartman number provokes heat and mass transfer to drop for various power-law indexes. However, the influence of external magnetic on double-diffusive natural convection of nanofluids has not been reported yet.

On the other hand, in the most of the available studies in the literature, streamlines, isotherms, and isoconcentrations are utilized to illustrate the fluid flow, temperature and concentration distributions, respectively. In fact, streamlines significantly present the fluid flow, whereas isotherms and isoconcentrations depict only temperature and concentration distributions which may not be adequate for the visualization of heat and mass transfer, respectively. The heatline visualization technique is developed recently to visualize the conductive as well as convective heat transfer of natural convection imposed by just temperature gradient. Basak & Chamkha (2012) utilized heatline visualization technique to study on natural convection in a square cavity filled with nanofluid. Biswal & Basak (2015) investigated the sensitivity of heat-function boundary conditions on the heatlines of natural convection in an enclosure with various wall heating. Alsabery *et al*. (2016) used heatline visualization to study natural convection in the cavity filled by nanofluid with sinusoidal temperature boundary conditions. Hussain (2016)

analyzed numerically heatlines of double-diffusive convection within a tilted sinusoidal corrugated porous enclosure in the presence of a magnetic field.

Similar to the heatline visualization technique, massline visualization technique would be a useful method to study mass transfer in double-diffusive natural convection problems. Masslines are mathematically represented by massfunctions which are in turn related to Sherwood number based on proper dimensionless form. However, there is no open literature available yet on masseline visualization of double-diffusive convection of nanofluids. Therefore, the main aim of the present contribution is to investigate double-diffusive natural convection in a square cavity filled with nanofluid in the presence of transverse magnetic field and heat flux utilizing massline visualization technique. As shown by the above literature convey, this problem has not been undertaken yet in the literature.

Moreover, double-diffusive natural convection of nanofluids is an important phenomena emerging in solar engineering equipment, such as collectors and solar water heaters, solar-thermal energy storage facilities, solar cell, and solar stills. It is sought that this work will contribute in finding new parameter arrangement which is helpful to deepen our insight into solar-thermal system optimization.

2. PROBLEM STATEMENT

The considered physical geometry with related parameters and coordinates is presented in Fig. 1. It consists of a two-dimensional lid-driven cavity with side equal to H, which elucidates the characteristic dimension of the problem. The heat source is centrally located on the bottom surface and its length is 3. The cooling is achieved by the right and left vertical walls which kept constant at minimum temperature T_l. The top and bottom wall except the heat source region are assumed adiabatic thermally. The heat source has a constant heat flux q'' during the sections 4-1 and 4-2, while it is enhanced by the heat flux coefficient ε in section 4-3. The right and left vertical walls have maximum and mini-mum concentrations, respectively ($C_h > C_l$), while the horizontal walls are assumed adiabatic solutally. The top moving lid has a constant velocity U0 towards the right. The applied external magnetic field has an inclination angle λ with x-axis, and was assumed constant B_0. The cavity is filled with Cu-water nanofluid. The thermo-physical properties of the base fluid and the nanoparticles are given in Table 1. The nanofluid used in the study is assumed to be incompressible and laminar, and the base fluid and suspended nanoparticles are in thermal equilibrium. Meanwhile, the single phase approach for nanofluid modelling is embraced. In this approach, the effects of addition of nanoparticles into the base fluid are considered by changing of the thermo-physical properties of the mixture (Kamyar *et al*. 2012, Chen *et al*. 2015). Viscous dissipation, Joule heating, and Hall effect are all assumed negligible. Moreover, the magnetic Reynolds number is assumed small enough, whereby magnetic field induction can be neglected. The thermo-physical properties of the nanofluid are assumed constant except for the density variation, which is examined based on the Boussinesq approximation. Introducing the following dimensionless set:

$$(X,Y)=\frac{(x,y)}{H},\ (U,V)=\frac{(u,v)}{U_0},\ P=\frac{p}{\rho_{nf}U_0^2},$$

$$\Theta=\frac{(T-T_l)}{q''H}k_{nf},\ \Phi=\frac{C-C_0}{C_h-C_l} \quad (1)$$

Table 1 Thermo-physical properties of pure water and copper nanoparticles

Physical properties	Pure water	copper
$\rho(kgm^{-3})$	997	8933
$C_p(Jkg^{-1}K^{-1})$	4179	385
$k(Wm^{-1}K^{-1})$	0.613	401
$\beta\times10^{-5}(K^{-1})$	21	1.67
$\sigma(Sm^{-1})$	0.05	596×10^7

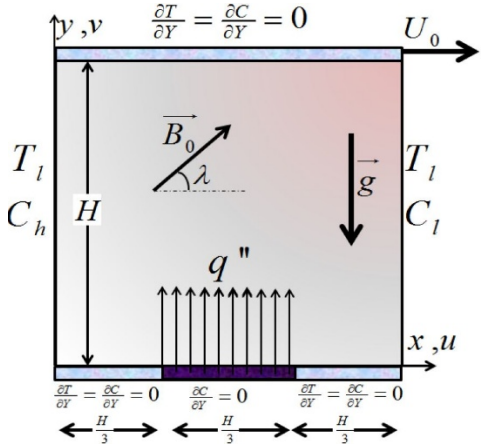

Fig. 1. Schematic configuration of the studied problem.

where C_0 and q'' are characteristic concentration and heat flux, respectively, the dimensionless form of the governing equations, including the continuity, momentum, energy, and concentration equations for the laminar steady-state double-diffusive natural convection can be written as (Esfahani & Bordbar, 2011, Chen *et al*. 2016):

$$\frac{\partial U}{\partial X}+\frac{\partial V}{\partial Y}=0 \quad (2)$$

$$U\frac{\partial U}{\partial X}+V\frac{\partial U}{\partial Y}=-\frac{\partial P}{\partial X}+\frac{1}{Re}\left(\frac{\nu_{nf}}{\nu_f}\right)\left(\frac{\partial^2 U}{\partial X^2}+\frac{\partial^2 U}{\partial Y^2}\right)+\left(\frac{\rho_f}{\rho_{nf}}\right)\left(\frac{\sigma_{nf}}{\sigma_f}\right)\frac{Ha^2}{Re}(Vsin\lambda cos\lambda-Ucos^2\lambda) \quad (3)$$

$$U\frac{\partial V}{\partial X}+V\frac{\partial V}{\partial Y}=-\frac{\partial P}{\partial Y}+\frac{1}{Re}\left(\frac{\nu_{nf}}{\nu_f}\right)\left(\frac{\partial^2 V}{\partial X^2}+\frac{\partial^2 V}{\partial Y^2}\right)+\left(\frac{\rho_f}{\rho_{nf}}\right)\left(\frac{\sigma_{nf}}{\sigma_f}\right)\frac{Ha^2}{Re}(Usin\lambda cos\lambda-Vcos^2\lambda)+Ri\frac{(\rho\beta)_{nf}}{\rho_f\beta_f}(\Theta+B\Phi) \quad (4)$$

$$U\frac{\partial\Theta}{\partial X}+V\frac{\partial\Theta}{\partial Y}=\frac{1}{RePr}\left(\frac{\alpha_{nf}}{\alpha_f}\right)\left(\frac{\partial^2\Theta}{\partial X^2}+\frac{\partial^2\Theta}{\partial Y^2}\right) \quad (5)$$

$$U\frac{\partial\Phi}{\partial X}+V\frac{\partial\Phi}{\partial Y}=\frac{1}{RePrLe}\left(\frac{\alpha_{nf}}{\alpha_f}\right)\left(\frac{\partial^2\Phi}{\partial X^2}+\frac{\partial^2\Phi}{\partial Y^2}\right) \quad (6)$$

The effective density at the reference temperature, thermal diffusivity, heat capacitance and thermal expansion coefficient of the nanofluids based on classical models can be found in Ghaffarpasand (2016). The effective thermal conductivity of nanofluid is approximated by the Maxwell self-consistent approximation model, whereby for the two-component entity of spherical-particle suspension, k_{nf} can be expressed as (Maxwell, 1983):

$$\frac{k_{nf}}{k_f}=\frac{k_s+2k_f+2\phi(k_f-k_s)}{k_s+2k_f+\phi(k_f-k_s)} \quad (7)$$

where ϕ is the solid volume fraction of the nanoparticles. The viscosity of the nanofluid is calculated using the Brinkman model as (Brinkman, 1952):

$$\mu_{nf}=\frac{\mu_f}{(1-\phi)^{2.5}} \quad (8)$$

The electrical conductivity of the nanofluid calculated by Maxwell model as (Maxwell, 1983):

$$\frac{\sigma_{nf}}{\sigma_f}=1+\frac{3(\xi-1)\phi}{(\xi+2)-(\xi-1)\phi} \quad (9)$$

where $\xi=\frac{\sigma_s}{\sigma_f}$. The problem of double-diffusive natural convection is characterized here by the following dimensionless parameters:

$$Ri=\frac{Gr_T}{Re^2}=\frac{g\beta\Delta TL^3/\nu_f^2}{(U_0L/\nu_f)^2},\ Pr=\frac{\nu_f}{\alpha_f},$$
$$Ha=B_0H\sqrt{\frac{\sigma_f}{\mu_f}},\ Le=\frac{Sc}{Pr},\ B=\frac{Gr_C}{Gr_T}$$

where Ri, Re, Ha, Pr, Le, Gr_T, and Gr_C are Richardson, Reynolds, Hartman, Prandtl, Lewis, thermal and solutal Grashof numbers, respectively, and B is the buoyancy ratio. The dimensionless boundary conditions are also given as:

U=1,V=0, $\frac{\partial\Phi}{\partial Y}=\frac{\partial\Theta}{\partial Y}=0$ (Top wall) (10)

U=V=0, Θ=0, $\Phi=1$ (Left wall) (11)

U=V=0, Θ=Φ = 0 (Right wall) (12)

U=V=0, $\frac{\partial\Phi}{\partial Y}=0$, (Bottom wall) (13)

$\frac{\partial\Theta}{\partial Y}=-\varepsilon\frac{k_f}{k_{nf}}, for\ \frac{1}{3}<X<\frac{2}{3}$, $\frac{\partial\Theta}{\partial Y}=0$, otherwise

The local Nusselt number along the heat source is examined as (Ismael *et al*. 2016, Sheikholeslami *et al*. 2016):

$$Nu_l=\frac{1}{\Theta\big|_{along\ Y=\frac{H}{3}:\frac{2H}{3}}} \quad (14)$$

and the average Nusselt number can be defined as:

$$\overline{Nu}=\left(\frac{3}{H}\int_{\frac{H}{3}}^{\frac{2H}{3}}Nu_l dY\right)_{X=0} \quad (15)$$

The local and average Sherwood number along the wall with maximum concentration can be expressed as:

$$Sh_l=\frac{\partial\Phi}{\partial X},\quad \overline{Sh}=\left(\int_0^1 Sh_l dy\right)_{Y=0} \quad (16)$$

As was mentioned before, one of the main aims of the study is using massline visualization technique to analyzed mass transfer across the cavity. For this purpose and in a method similar to Hooman (2007), the scaled massfunction M, scaled by $(C_h-C_l)k_f$, is given by:

$$\frac{\partial M}{\partial Y}=U\Theta-\left(\frac{1}{RePrLe}\frac{\alpha_{nf}}{\alpha_f}\right)\frac{\partial\Phi}{\partial X} \quad (17)$$

$$-\frac{\partial M}{\partial X}=V\Theta-\left(\frac{1}{RePrLe}\frac{\alpha_{nf}}{\alpha_f}\right)\frac{\partial\Phi}{\partial Y} \quad (18)$$

The first and second terms of the right hand side of the Eqs. (17)&(18) represent, respectively, the convective and conductive mass fluxes along x,y directions. The massfunction M satisfies the following Poisson equation:

$$\nabla^2M=RePrLe\frac{(\rho C_P)_{nf}}{(\rho C_P)_f}\left[\frac{\partial(U\Phi)}{\partial Y}-\frac{\partial(V\Phi)}{\partial X}\right] \quad (19)$$

The massfunction is determined by solving the above Poisson equation subjected to the boundary conditions. It's worthwhile to note that the non-homogenous Dirichlet boundary condition was implied with the massfunction.

NUMERICAL SOLUTION

The governing Eqs. (2)-(6) subjected to the boundary conditions (Eqs. 10-13) are solved numerically using an accurate finite difference method. The central difference and first upwind approaches have been utilized to estimate the diffusive and convective terms, respectively. The resulting discretized equations have been solved using the SIMPLE algorithm (Patankar, 1980). In this study, several grid testings are performed for different uniform grids, namely, 100×100, 128×128, and 140×140, and for a typical case dealing with ϕ = 0.1 and Ri = 10. Minor differences of less than 0.3% detected between produced results by different used grids. Therefore, considering simulated accuracy and CPU time in the range of variables, the uniform grid of 128 × 128 found enough fine to ensure the grid independent solution. The convergence criterion for the termination is also implemented, whereby the following criterion was satisfied for all computations:

$$\max_{grid}\left|\Gamma^{S+1}-\Gamma^{S}\right|\le 10^{-7} \quad (20)$$

where s is the iteration number and Γ stands for the set of U, V , Θ, and Φ. In order to verify the accuracy of the present method, the code is validated with the former published results in three steps. First, the average Nusselt number for natural convection in the absence of applied magnetic field and heat flux was evaluated and compared with the existence benchmark results available in the literature in Table 2. As can remark, a good agreement is seen between the results of the present method and available in the

Table 2 Comparison of the average Nusselt numbers for natural convection of pure air

Ra	10^4	10^5
Hortmann et al. (1990)	2.245	4.522
Ismail & Scalon (2000)	2.256	4.651
Barakos & Mitsoulis (1994)	2.245	4.510
Present study	2.257	4.611

benchmarks. Then the average Nusselt number on the bottom wall with a constant heat flux for cavity inclination angle equals to zero, dimensionless length of the heat source 0.6, and two Grashof numbers, i.e. Gr = 10^3 and 10^5, were calculated and compared with the results of Sheikholeslami *et al.* (2016) in Fig. 2(a). In further, the variation of the average temperature at the mid plane of the cavity for natural convection of Cu-water nanofluid for Gr = 10^4 and ϕ = 0.1 was computed and compared with the results of Khanafer *et al.* (2003) in Fig. 2(b). All the comparisons show an acceptable agreement between the results obtained by the present method and the previous works.

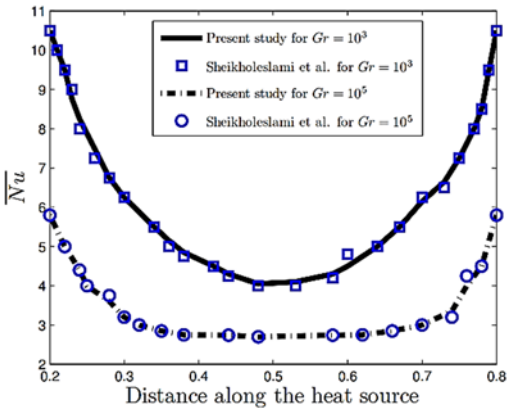

(a)

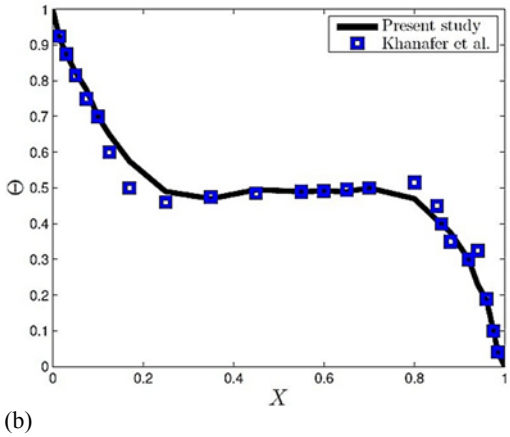

(b)

Fig. 2. (a) Comparison of the average Nusslet number between the present results and numerical results by Sheikholeslami *et al.* (2016), (b) comparison of the average temperature on the mid plane of the cavity obtained by the present method and results of Khanafer *et al.* (2003), when Gr = 10^4, and ϕ = 0.1.

3. RESULTS AND DISCUSSIONS

Masslines, isoconcentrations, isotherms, the average Nusselt and Sherwood numbers are adopted in inspecting the results of double-diffusive natural convection aspects of the present problem. The studied parameters which pertinently affect the flow, solutal and thermal fields inside the investigated enclosure are the orientation angle of the magnetic field $\lambda = 0^\circ - 270^\circ$, Hartman number Ha = 0−100, heat flux coefficient ε = 1−200, and solid volume fraction of nanoparticles ϕ = 0−10%. Prandtl number, Richardson number, the size and position of the heat source are all kept constant during this study, whereby Pr = 6.8, and Ri = 10. It is worthwhile to note that both of Lewis number and buoyancy ratio are set to unity during this study. This implies similar diffusion characteristics for both of heat and mass transfer and facilitates highlighting the implications of studied pertinent parameters. For the purpose of viewing the results easily, three parameters are kept constant (unless where stated), while the reminder single one is varied. The results and discussions are illustrated in the following categories.

4.1 Effect of Magnetic Field Orientation λ

We firstly investigate the effect of orientation angle of applied magnetic field (λ), while the other parameters are fixed at ε = 1, and Ha = 25. Fig. 3 shows the distributions of masslines, isoconcentrations, and isotherms for various values of λ and two values of ϕ, i.e. ϕ = 0 and 5%. For all of those, going from left to right the λ is varied from 0° to 270°. One can observe that the masslines are formed in a main clockwise circulation which occupied whole the cavity. The masslines start and terminate at the left and right walls with maximum and minimum concentrations, respectively. In the bottom half of the cavity and near the heat source, the mass flux vectors follow a closed loop. It may be noted that the mass flux vectors are tangential to the masslines. However, the appearance of closed loop elucidates the dominance of convective mass transfer in that region. As the orientation angle of applied magnetic field increases to $\lambda = 90^\circ$, the circulation becomes strong due to enhance in convective mass transfer.

It is well-known that applying an external magnetic field will be produced a familiar force, Lorenz force, perpendicular to the direction of the applied magnetic field. When $\lambda = 0^\circ$, Lorenz force will act normally in the negative Y-direction, i.e. opposite to the thermal buoyancy force. Hence, with increasing

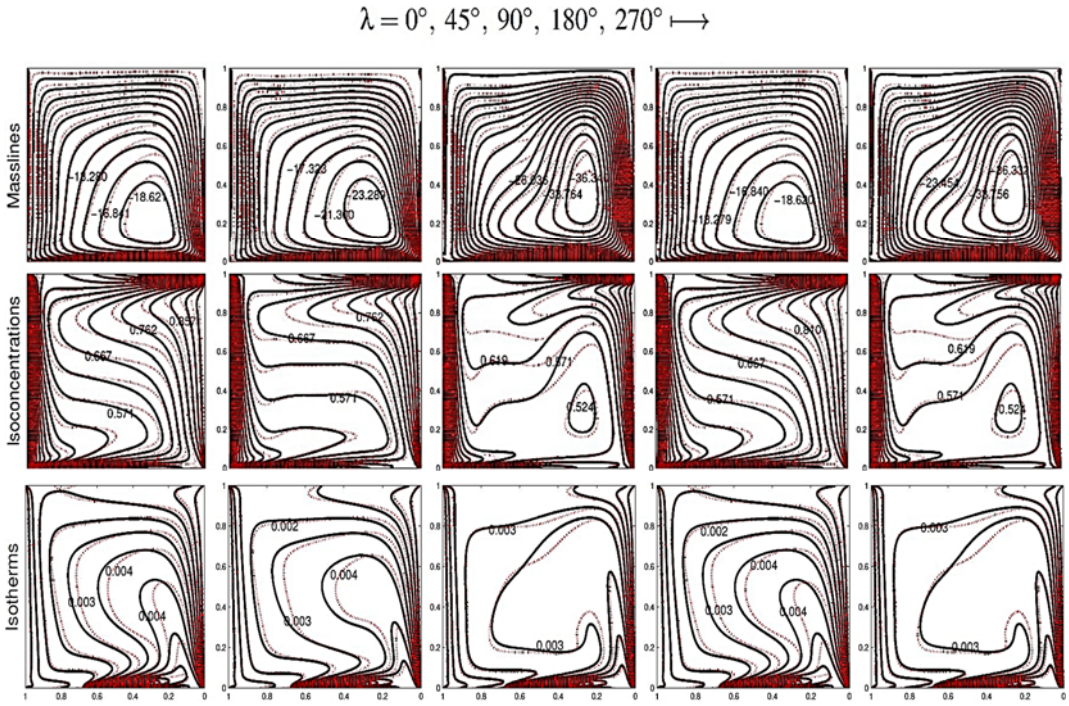

Fig. 3. Masslines, isoconcentrations, and isotherms for Ha = 25, and ε = 1. Dotted lines are for pure fluid (ϕ = 0) and solid lines are for nanofluid (ϕ = 5%).

λ to 90°, the opposite action of Lorenz force against the thermal buoyancy force attenuates, as a result the masslines strength increases. When λ is increased to 180° and then 270°, the magnetic force will act downward and horizontally, the cases which are identical to be that of λ = 0° and 90°, respectively. The massline distributions also indicate that the size of vortices decreases with an increase of solid volume fraction of nanoparticles.

It is well-known that adding high conductive solid nanoparticles produces a nanofluid with higher viscosity, density and thermal conductivity than the pure fluid (Ismael *et al.* 2016). The first two properties improve the viscous and inertial forces, correspondingly, while the increased thermal conductivity enhances the transferred thermal energy. However, increasing fluid friction due to adding nanoparticles reduces mass transfer across the cavity, whereby nanofluid has smaller masslines circulation vortices with respect to the pure fluid (ϕ = 0). Fig. 3 also presents the influence of orientation angle of applied magnetic field on isoconcentrations and isotherms. It can be seen that the thickness of solutal boundary layer and so the convective mass transfer increase as λ enhances to 90°. Besides, the strength of isotherm lines at the core of the cavity was reduced by increasing λ to 90°. This fact illustrates that temperature gradient within the cavity decreases as λ increases to 90°. Meanwhile, the cases with λ = 180° and 270° have almost similar iso-concentration and isotherm patterns with cases with λ = 0°&90°, respectively. This fact is due to the direction of generated Lorenz force, explained before. However, the isoconcentration and isotherm contours of pure fluid (dotted lines) take the same behavior of the isoconcentrations and isotherms of nanofluid (solid lines). Nevertheless, the solutal and thermal gradients of nanofluid across the cavity are usually smaller and larger, respectively, than the pure fluid case. The presence of high thermal conductive nanoparticles with larger density than pure fluid reduces mass transfer on one side, and enhances the heat transfer of the nanofluid on the other side.

The average Nusselt and Sherwood numbers are plotted with the orientation angle of applied magnetic field for different values of ϕ in Fig. 4. It should be reminded that the average Nusselt number was calculated on the heat source at the bot-tom horizontal wall. First, a sinusoidal behavior was observed in all figures. This fact is attributed to the similar direction of generated Lorenz force in cases with λ = 0°&180°, and λ = 90° and 270°, explained before, which obtained almost identical values of the average Nusselt and Sherwood numbers. As was depicted in Fig. 4(a)&(b), it's evident that Nu and Sh have their minimum and maximum values when λ = 90°, respectively. These figures also represent that the average Sherwood number in comparison with the average Nusselt number is sensitive greatly to the orientation angle variation. It can also be seen that all of the average Nusselt and Sherwood numbers are increased and decreased with further enhancement of solid volume fraction of nanoparticles, respectively. In other words, adding metallic nanoparticles with relatively larger thermal conductivity and larger density than the pure fluid in the presence of a magnetic field with a moderate strength increases thermal conductivity and

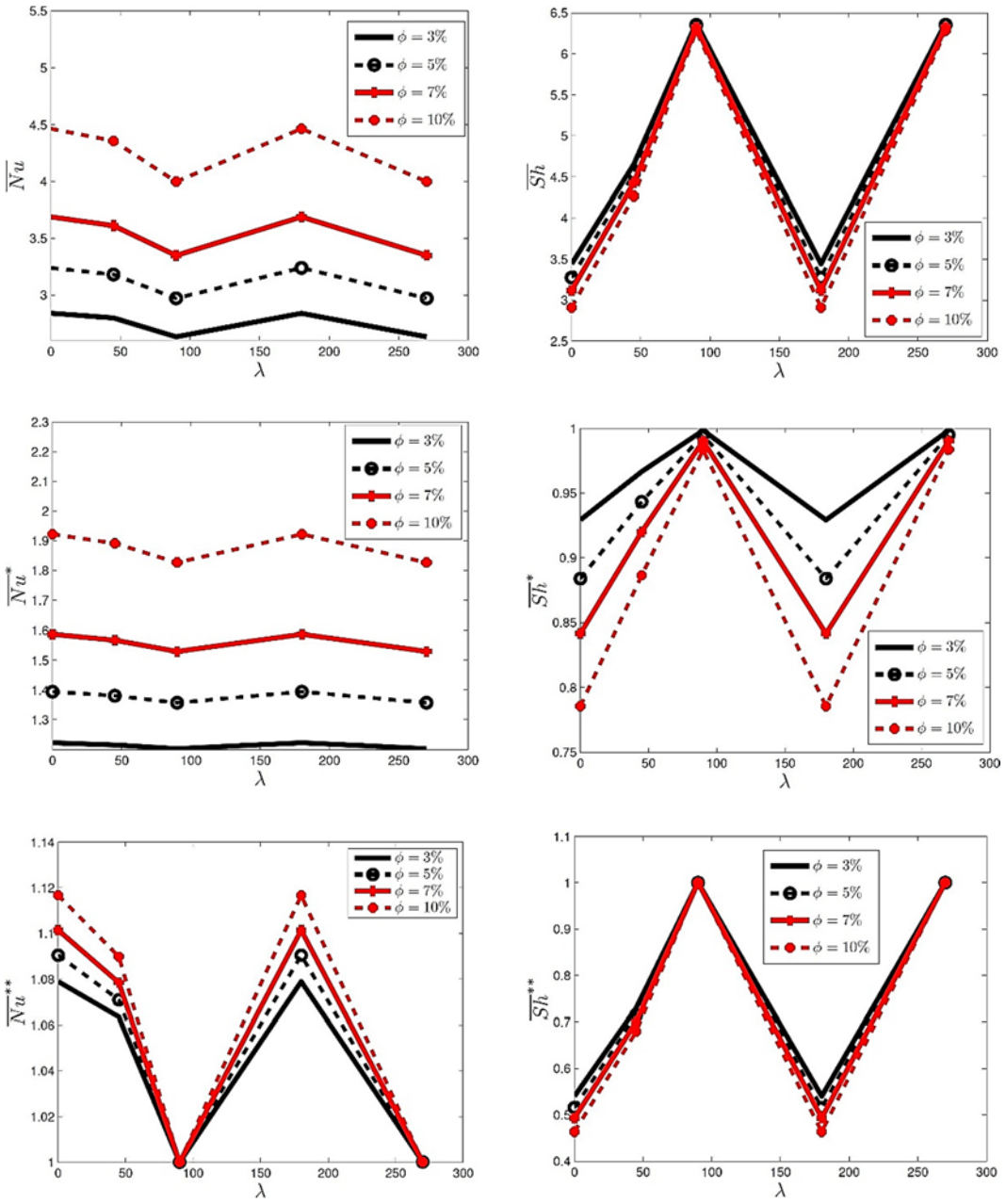

Fig. 4. Variation of (a) average Nusselt number, (b) average Sherwood number, (c) $\overline{Nu}^*$, (d) $\overline{Sh}^*$, (e) $\overline{Nu}^{**}$, and (f) $\overline{Sh}^{**}$ with orientation angle of applied magnetic field for various solid volume fraction where Ha = 25, and ε = 1.

viscosity of nanofluid which result in increasing and decreasing the heat and mass transfer, respectively.

The variation in rates of the average Nusselt and Sherwood numbers due to adding nanoparticles and applying external magnetic field are presented in Fig. 4(c)-(f). Fig. 4(c) shows that the heat transfer enhancement due to adding nanoparticles reduces with further enhancement of λ up to 90°. Moreover, the heat transfer enhancement was augmented with adding more volume fraction of nanoparticles. Fig. 4(d) represents that the orientation angle of applied magnetic field is an important factor in mass transfer reduction due to adding nanoparticles, whereby the influence of solid volume fraction on mass transfer reduction was attenuated with further enhancement of λ to 90°. Fig. 4(e) indicates that the external magnetic field causes an enhancement in the average Nusselt number, whereby all of the values $\overline{Nu}^{**}$ are larger than unity. The average Nusselt number was calculated on the heat source at the horizontal bottom wall. Hence, applying the external magnetic field with λ = 0°&180° has an opposing action against the thermal buoyancy force and so formed the concentrated thermal boundary layers near the heat source. This fact causes an enhancement in the computed average Nusselt number. In contrast, the convective current of energy was attenuated to some

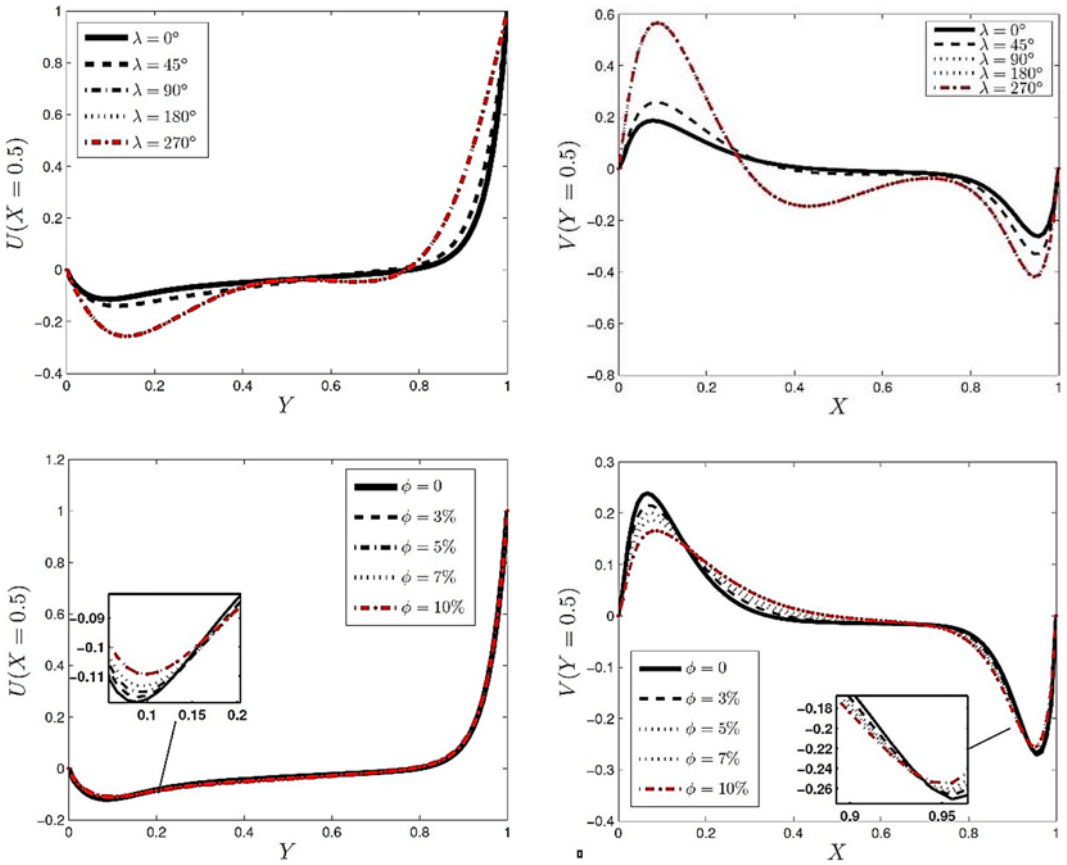

Fig. 5. (a) Horizontal and (b) vertical velocities along mid sections of the enclosure for various orientation angles where Ha = 25, ϕ = 5%, and ε=1; (c) horizontal and (d) vertical velocities along mid sections of the enclosure for various volume fractions of nanoparticles where Ha = 25, λ=45°, and ε=1.

extent in those cases, and so convective mass transfer Sh, was reduced significantly in cases with λ = 0°&180°, as can be seen in Fig. 4(f).

The influence of the orientation angle of magnetic field and solid volume fraction of nanoparticles on velocity components are illustrated in Fig. 5. In these figures, the horizontal U and vertical V velocity components are plotted along Y = 0.5, and X = 0.5, respectively. Fig. 5(a) elucidates that the U component reveals negative values close to the bottom wall which means that buoyancy effect is dominant in that region. Therefore, the cases with λ=0° has maximum values of U velocity near the bottom wall. As can be observed in Fig. 5(b), two peaks of the vertical components V are recorded close to the vertical walls with higher velocity values associated with increasing λ. This result resembles the results of Ismael *et al.* (2016), where the influence of partial slip and inclined magnetic field on the mixed convection of nanofluid was studied numerically.

Fig. 5 (c) represents that the influence of solid volume fraction on the variation of U velocity component seems to be insignificant. Nevertheless, near the bottom horizontal walls, nanofluids with larger ϕ values have larger U velocity components. It seems that the existence of larger volume fraction of metallic nanoparticles in the pure fluid cause that nanofluid is affected greatly by heat source of the bottom wall. Fig. 5(d) indicates that nanofluids with larger ϕ values have smaller V velocity components near the vertical walls, while the opposite was observed at the core of the cavity. The fluid resistance increases as the distance from the wall reduces. Moreover, fluid friction and nanofluid viscosity are enhanced with increasing ϕ value. Therefore, nanofluid with larger ϕ values have smaller V velocity component near the wall. On the other hand, at the core of the cavity and when the wall effect is attenuated greatly, nanofluids with larger volume fraction of high electrical conductive nanoparticles are affected to some extent by the external magnetic field and so have larger V velocity components.

4.2 Effect of Hartman Number Ha

The effect of applied magnetic field is investigated by varying the Hartman number from zero to 100, when λ = 0° and the heat flux coefficient is fixed at unity. Effect of Hartman number on masslines, isoconcentrations, and isotherms are depicted in Fig. 6. As was mentioned before, Lorenz force will be generated perpendicular to the direction of the applied magnetic field, i.e. in the negative Y-direction here. Therefore, Lorenz force will act

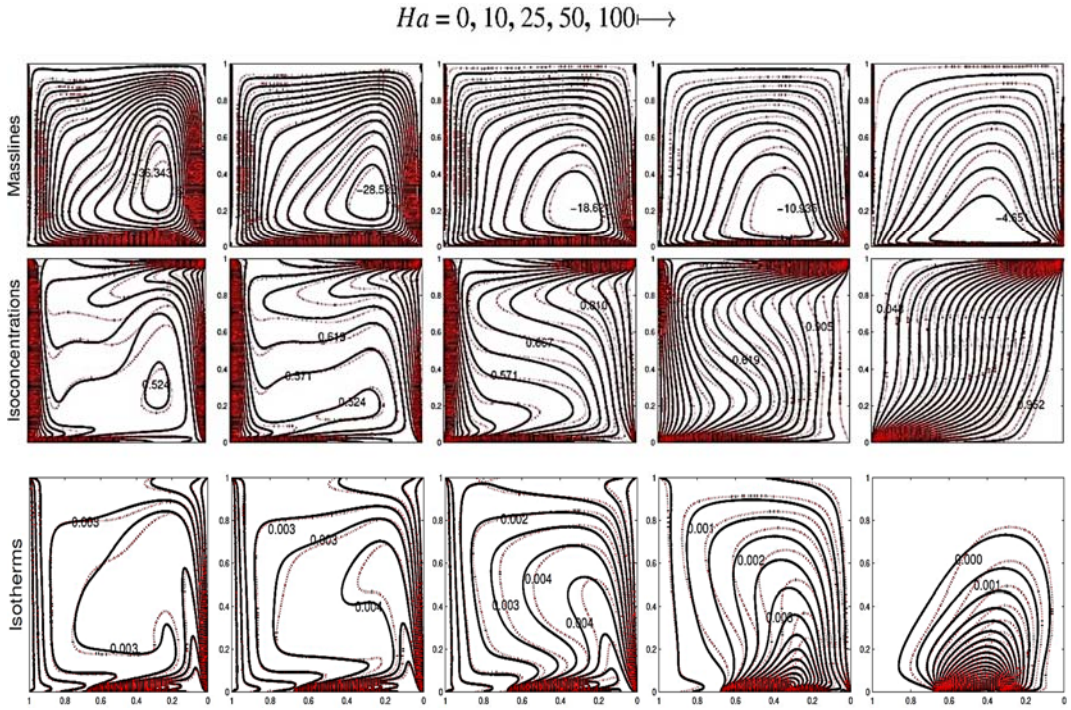

Fig. 6. Masslines, isoconcentrations, and isotherms for λ = 0°, and ε = 1. Dotted lines are for pure fluid (ϕ = 0) and solid lines are for nanofluid (ϕ = 5%).

opposite to the thermal buoyancy force. Accordingly, the strength of masslines circulation was attenuated with further increase of Hartman number. Moreover, it can be seen that the main clockwise circulation of masslines pushes downward with increase of Hartmann number. Similar to the previous section, nanofluid has smaller closed loops with respect to the pure fluid. Isoconcentration patterns are also became parallel to vertical walls with increase of Hartman number. In small values of Hartman number, isotherms tend to be plumed from heat source towards the cold vertical walls with isothermal zones localized close the vertical walls and dense isotherms close to the heat source.

With increasing Hartman number, and so increasing opposite action of Lorenz force against the thermal buoyancy force, thermal plume over the bottom wall omits. Increasing the concentration of isothermal lines near the heated source with increasing Ha value enhances the temperature gradient in that region and so caused an enhancement in the average Nusselt number, as shown in Fig. 7(a). It is obvious that nanofluids with larger volume fraction of high conductive nanoparticles have larger Nu values. As was observed in Fig. 6, the convective distortion of isoconcentration lines was reduced with the increase of Hartman number, whereby the conductive mode of mass transfer dominates significantly convective mass transfer in cases with largest Hartman number. This fact is also confirmed in Fig. 7(b), where the average Sherwood number is a decreasing function of Hartman number. However, for small and moderate Hartman numbers (Ha ≤ 50), adding solid nanoparticles with relatively larger density than the base fluid, increases nanofluid viscosity and so reduces Sh values. On the other hand, in cases under strengthened magnetic field (Ha = 100), adding more volume fraction of high electrical conductive nanoparticles causes an enhancement in convective mass transfer across the cavity. It seems that increasing electrical conductivity of the nanofluid in presence of external magnetic field has an aiding effect on convective mass transfer within the cavity. The variation in rates of the average Nusselt and Sherwood numbers due to adding nanoparticles as a function of Hartman number are depicted in Fig. 7(c)&(d), respectively. It can be seen that the value of $\overline{Nu}^*$ increases slightly with increase of the Ha up to 25 and then it reduces with further enhancement of Hartman number. It seems that the existence of high electrical conductive nanoparticles in presence of the strengthen external magnetic field augments and attenuates the conductive and convective mode of heat transfer, respectively. As can be observed in Fig. 7(d), combined effect of strengthen external magnetic field and the existence of nanoparticles also causes an enhancement in $\overline{Sh}^*$ values in larger Hartman numbers. Fig. 7(e) and (f) represents that the U component is flattened with Ha, while the peaks of V component are greatly vanished with increasing Hartman number. In other words, when the external magnetic field is applied on the cavity the velocity field suppressed, owing to the retarding effect of the Lorenz force. The suppression effect of Lorenz force against fluid flow characteristics was observed and discussed by many previous investigators, e.g. Sheikholeslami *et al.* (2016), Hussain (2016), and Kefayati (2016).

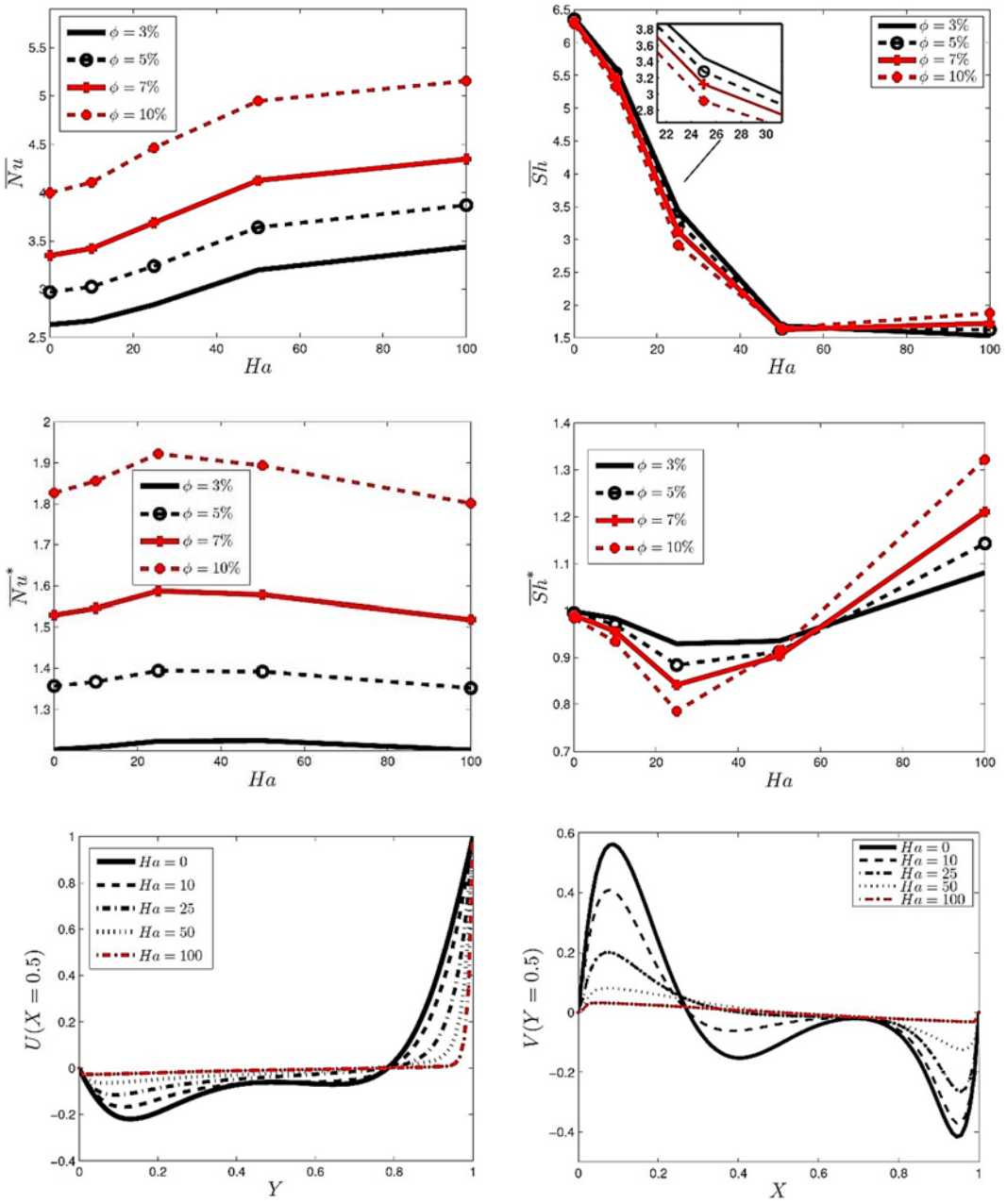

Fig. 7. Variation of (a) average Nusselt number, (b) average Sherwood number, (c) $\overline{Nu}^*$, (d) $\overline{Sh}^*$, with Hartman number for various solid volume fractions and (e) horizontal, and (f) vertical velocities along mid sections of the cavity where Ha = 25, and ε = 1.

4.3 Effect of Heat Flux Coefficient ε

The effect of heat flux coefficient will be discussed in this category for Ha = 25, and λ = 0°. As was mentioned before, heat flux was enhanced by the factor of ε, named heat flux coefficient. Fig. 8 shows the effect of ε on the masslines, isoconcentrations, and isotherms. It can be seen that when ε is increased to 50, the main clockwise circulation of masslines is weaken and secondary vortex is began to form close to the moving top wall. Nevertheless, the massfunction value increases with increasing ε to 50. The strength of secondary anticlockwise circulation was augmented with further enhancement of ε value, while the opposite was observed for the strength of clockwise primary circulation. The anti-clockwise circulation was formed by injecting high amount of heat flux through the cavity. A same observation was observed in the study of Ismael *et al.* (2016), when Richardson number as the ratio of natural to forced convection modes was reduced. Interestingly, the size of the massline secondary circulation of pure fluid is still larger than the size of nanofluid secondary circulation. In other words, the size of massline vortices is reduced with adding minor volume fraction of nanoparticles.

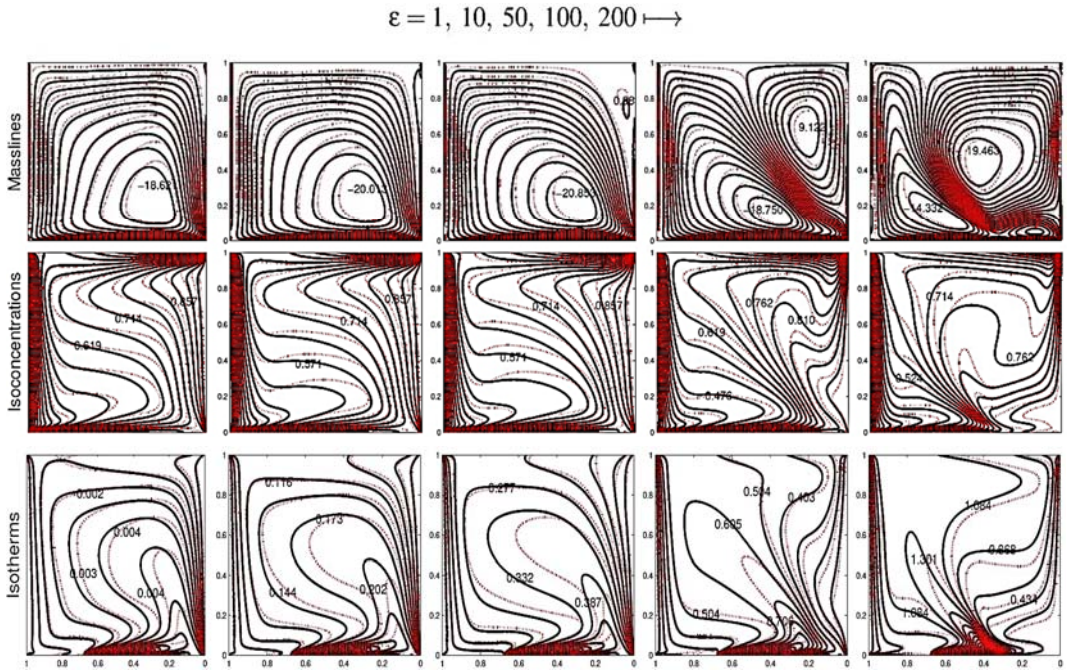

Fig. 8. Masslines, isoconcentrations, and isotherms for Ha = 25, and λ = 0°. Dotted lines are for pure fluid (ϕ = 0) and solid lines are for nanofluid (ϕ = 5%).

Figure 8 presents that isoconcentration has an almost undistributed pattern with increasing ε to 50, while isoconcentration distortion was increased with further enhancement of ε value. This fact indicates that the convective mass transfer was improved by increasing ε from 50. It can also be seen that the isotherm line values were enhanced with increasing heat flux coefficient. This feature clearly elucidates that heat penetrates much deeper into the cavity with increasing ε value.

Figure 9(a) shows that the concentration of thermal boundary layer near the heat source, the average Nusselt number, was reduced with increasing ε value. Meanwhile, the influence of solid volume fraction on Nu seems to be insignificant. The variations of the average Sherwood number as a function of heat flux coefficient for various volume fraction of nanoparticles are illustrated in Fig. 9(b). As can be seen, the average Sherwood number was slightly reduced with increasing ε to 100 and then it was monotonically increased with further enhancement of heat flux coefficient. It seems that for small and moderate values of ε (ε ≤ 100), the extra injected heat flux decreases mass transfer within the cavity. In contrast, the extra heat injected through the cavity in cases with larger ε values has an aiding effect on mass transfer across the cavity. The variations of $\overline{Nu}^{*}$, $\overline{Sh}^{*}$, $\overline{Nu}^{**}$, and $\overline{Sh}^{**}$ as a function of ε are depicted in Figs. 9(c)-(f). Fig. 9(c) shows that heat flux coefficient has an insignificant effect on the heat transfer enhancement due to adding nanoparticles, whereas nanofluids with larger ϕ values have still larger heat transfer enhancement rates. Fig. 9(d) elucidates that the value of mass transfer reduction due to adding nanoparticles $\overline{Sh}^{*}$, decreases slightly with increasing ε to 100, and then it in-creases with further enhancement of ε. Fig. 9(e) shows the variation of average Nusselt number enhancement due to applied magnetic field as a function of heat flux coefficient. As can be seen that increasing heat flux coefficient causes an enhancement in $\overline{Nu}^{**}$. Meanwhile, the cases with larger φ values have larger $\overline{Nu}^{**}$ values. Fig. 9(f) shows that the variation of $\overline{Sh}^{**}$ as a function of ε is fairly similar to the variation of $\overline{Sh}^{*}$ values. In other words, the high extra heat injected through the cavity attenuates suppression effects of adding nanoparticles and applying external magnetic field against convective mass transfer across the cavity. The horizontal U and vertical V velocity components are plotted in Figs. 9(g) and (h), along Y = 0.5, and X=0.5, respectively. It can be seen that increasing heat flux co-efficient causes an enhancement and a reduction in horizontal and vertical components of velocity near the walls, respectively. Meanwhile, at the highest values of ε, the cavity center (core center) is not appearing as stagnant point.

4. SUMMARY AND CONCLUSIONS

In this paper, massline visualization technique was utilized for the first time to investigate the double-diffusive natural convection in a square cavity filled with Cu-water nanofluid and in the presence of an external transverse magnetic field. The main objective was to explore combined effects of the orientation angle and strength of applied magnetic field, heat flux coefficient, and volume fraction of solid nanoparticles on the thermal and solutal behavior of nanofluid as well as the heat and mass transfer across the cavity. The finite difference method was applied to solve the dimensionless

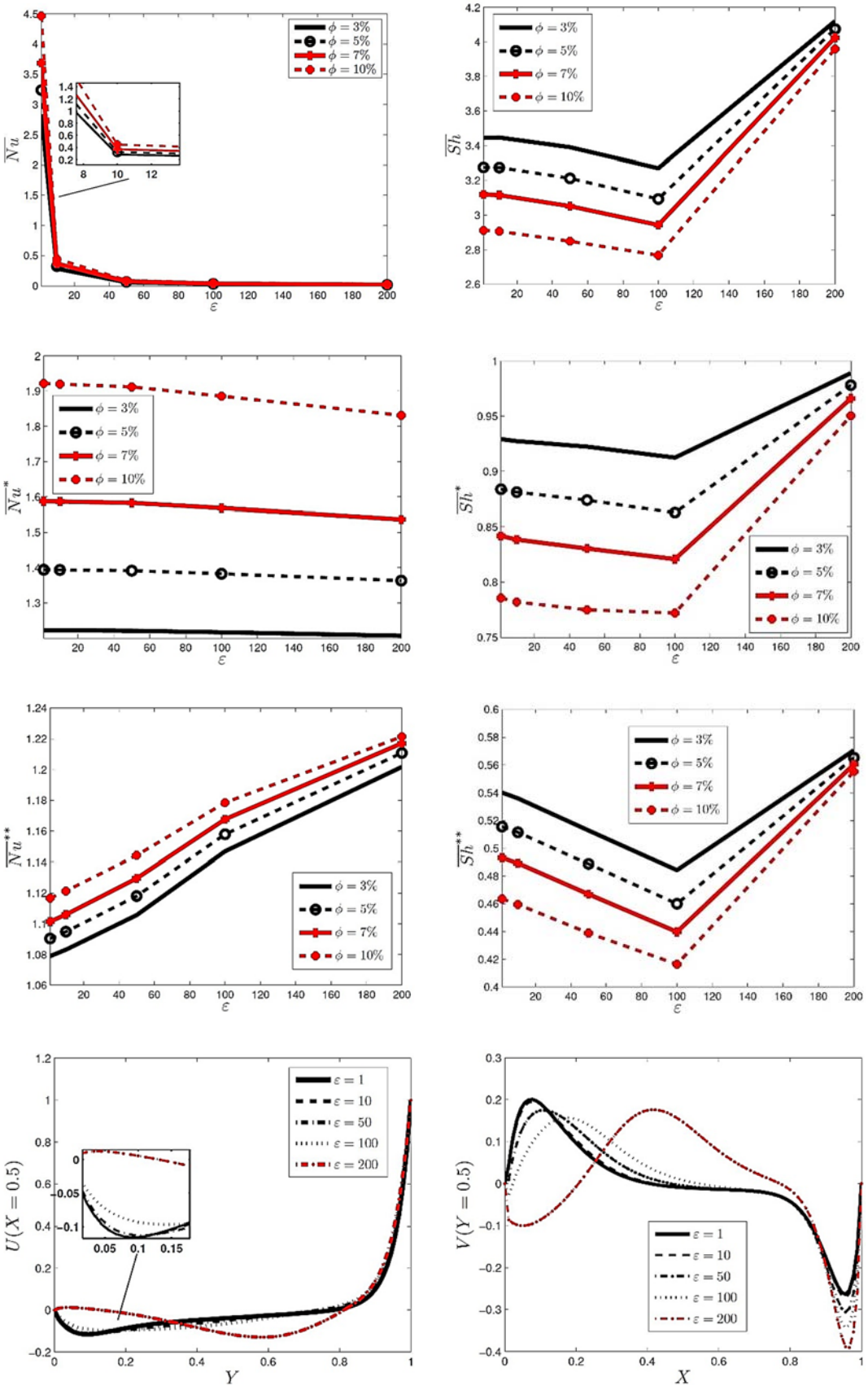

Fig. 9. Variation of (a) average Nusselt number, (b) average Sherwood number, (c) $\overline{Nu}^{*}$, (d) $\overline{Sh}^{*}$, (e) $\overline{Nu}^{**}$, and (f) $\overline{Sh}^{**}$ with heat flux coefficient for various solid volume fractions; (g) horizontal and (h) vertical velocities along mid sections of the enclosure for various heat flux coefficients (ϕ = 5%), where Ha = 25, and λ=0°.

governing equations together with the appropriate boundary conditions. In view of the above study the following conclusions are outlined:

1. The orientation angle of external applied magnetic field can play an important role in controlling double-diffusive natural convection, whereby the average Nusselt and Sherwood numbers are decreased and increased with increasing the orientation angle of the applied magnetic field, respectively.
2. Adding metallic nanoparticles with relatively larger thermal conductivity and density than the pure fluid enhances both of the nanofluid thermal conductivity and fluid friction. The first property causes an enhancement in the average Nusselt number, while the second one makes a reduction in the mass transfer across the cavity.
3. Pure fluid has relatively larger massline circulation loops than nanofluid. This fact is due to the increase of nanofluid viscosity due to adding nanoparticles.
4. The effect of the nanoparticles volume fraction in the presence of applied magnetic field manifests wide variety fashions, where in cases under magnetic fields with low and moderate strength, adding nanoparticles enhances fluid friction and reduces the average Sherwood number. In contrast, in cases under strengthened magnetic field, the presence of high electrical conductive nanoparticles has an aiding effect on mass transfer within the cavity.
5. Injecting high amount of heat flux through the cavity has an aiding effect on the convective current of mass transfer.

REFERENCES

Al-Amiri A., K. Khanafer, K., J. Bull and I. Pop (2007). Numerical simulation of combined thermal and mass transport in a square lid-driven cavity. International *Journal of Thermal Science 46*, 662-671.

Alim, M. A. and R. Nasrin (2013). Modelling of double-diffusive buoyant flow in a solar collector with water-CuO nanofluid. *Heat Transfer-Asian Research 42*, 212-229.

Alsabery, A. I., A. J. Chamkha, S. H. Hussain, H. Saleh and I. Hashim (2016). Heatline visualization of conjugate natural convection in a square cavity filled with nanofluid with sinusoidal temperature variations on both horizontal walls. International *Journal of Heat and Mass Transfer 100*, 835-850.

Aly, AM. and Z. A. S. Raizah (2016). Double-diffusive natural convection in an enclosure filled with nanofluid using ISPH method. *Alexandria Engineering Journal 55*, 3037-3052.

Barakos, G. and E. Mitsoulis (1994). Natural convection flow in a square cavity revisted: laminar and turbulent models. *International Journal of Numerical Method in Heat and Fluid Flow 18,* 695-719.

Basak, T. and A. J. Chamkha (2012). Heatline analysis on natural convection for nanofluids confined with square cavities with various thermal boundary conditions. *International Journal of Heat and Mass Transfer 55*, 5526-5543.

Biswal, P. and T. Basak (2015). Sensitivity of heatfunction boundary conditions on invariance of Bejan's heatlines for natural convection in enclosures with various wall heatings. *International Journal of Heat and Mass Transfer 89*, 1342-1368.

Brinkman, H. C. (1952). The viscosity of concentrated suspensions and solutions. *Journal of Chemical Physics 20*, 571-581.

Chen, Sh., B. Yang, X. Xiao and Ch. Zheng (2015). Analysis of entropy generation in double-diffusive natural convection of nanofluid. *International Journal of Heat and Mass Transfer 87*, 447-463.

Choi, S. U. S. (1995). Enhancing thermal conductivity of fluid with nanoparticles. *ASME Fluid Engineering Division 23*, 99-105.

Esfahani, J. A. and V. Bordbar (2011). Double diffusive natural convection heat transfer enhancement in a square enclosure using nanofluids. *Journal of Nanotechnology in Engineering Medicine 2*, 0210021-9.

Ghaffarpasand, O. (2016). Conjugate effect of Joule heating and unsteady MHD natural convection in a differentially heated skewed porous cavity saturated by Cu-water nanofluid. *Journal of Applied Fluid Mechanic* 9(6), 2823-2836.

Hooman, K. (2010). Energy flux vector as new tool for convection visualization. *International Journal of Numerical Method in Heat and Fluid Flow 20*, 240-249.

Hortmann, M., M. Peric and G. Scheuener (1990). Finite volume multigrid prediction of laminar natural convection: bench-mark solutions. *International Journal of Numerical Method in Heat and Fluid Flow 11*, 189-207.

Hussain, S. H. (2016). Analysis of heatlines and entropy generation during double-diffusive MHD natural convection within a tilted sinusoidal corrugated porous enclosure. *International Journal of Engineering Science and Technology, 19*, 926-945.

Ismael, M. A., M. A. Mansour, A. J. Chamkha and A. M. Rashad (2016). Mixed convection in a nanofluid filled-cavity with partial slip subjected to constant heat flux and inclined magnetic field. *Journal of Magnetism and Magnetic Material 416*, 25-36.

Ismail, K. A. R. and V. L. Scalon (2000). A finite element free convection model the side wall heated cavity. *International Journal of Numerical Method in Heat and Fluid Flow 43*, 1373-1389.

Jena Sofen,K., L. K. Malla, S. K. Mahapatra and A. J. Chamkha (2015). Transient buoyancy-opposed double diffusive convection of micropolar fluids in a square enclosure. *International Journal of Heat and Mass Transfer 81*, 681-694.

Kamyar, A., R. Saidur and M. Hasanuzzaman (2012). Application of computational fluid dynamics (CFD) for nanofluids. *International Journal of Heat and Mass Transfer 55*, 4104-4115.

Khanafer, K., K. Vafai and M. Lightstone (2003). Buoyancy-driven heat transfer enhancement in a two-dimensional enclosure utilizing nanofluids. *International Journal of Heat and Mass Transfer 19*, 3639-3653.

Kefayati, Gh. R. (2016). Simulation of double-diffusive MHD (magnetohydrodynamics) natural convection and entropy generation in an open cavity filled with power-law fluids in the presence of Soret and Dufour effects (Part I: study of fluid flow, heat and mass transfer). *Energy 107*, 889-916.

Maxwell, J. C. (1983). *A Treatise on Electricity and Magnetism*. vol. II, Oxford University Press, Cambridge, UK.

Mondal, S. and P. Sibanda (2015). Unsteady double diffusive convection in an inclined rectangular lid-driven enclosure with different magnetic field angles and non-uniform boundary conditions. *International Journal of Heat and Mass Transfer 90*, 900-910.

Parvin, S., R. Nasrin, M. A. Alim and N. F. Hossain (2012). Double diffusive natural convection in a partially heated enclosure using nanofluids. *Heat Transfer-Asian Research 41*, 484-497.

Patankar, S. V. (1980). *Numerical heat transfer and fluid flow*. Hemisphere, Washington D. C.

Qin, Q., Z. A. Xia and Z. F. Tian (2014). High accuracy numerical investigation of double diffusive convection in a rectangular enclosure with horizontal temperature and concentration gradients. *International Journal of Heat and Mass Transfer 71*, 405-423.

Schmit, R. W. (1994). Double diffusion in oceanography. *Annual Review of Fluid Mechanic 2*6, 255-265.

Sheikholeslami, M., T. Hayat and A. Alsaedi (2016). MHD free convection of Al2O3-water nanofluid considering thermal radiation: A numerical study. *International Journal of Heat and Mass Transfer 96*, 513-524.

Wang L., B. Shi, Z. Chai and X. Yang (2016). Regularized lattice Boltzmann model for double-diffusive convection in vertical enclosures with heating and salting from below. *Applied Thermal Engineering 103*, 365-376.